Laboratory experiments on Alfvén waves caused by rapidly expanding plasmas and their relationship to space phenomena

W. Gekelman, M. Van Zeeland, S. Vincena, and P. Pribyl

Department of Physics and Astronomy, University of California, Los Angeles, California, USA

Received 18 October 2002; revised 8 March 2003; accepted 19 March 2003; published 10 July 2003.

[1] There are many situations which naturally occur in space (coronal mass ejections, supernovas) or are man-made (upper atmospheric detonations) in which a dense plasma expands into a background magnetized plasma that can support Alfvén waves. The Large Plasma Device (LAPD) at UCLA is a machine in which Alfvén wave propagation in homogeneous and inhomogeneous plasmas has been studied. A new class of experiments which involve the expansion of a dense (initially $n_{\text{laser-produced}}/n_{\text{background}} \gg 1$) laser-produced plasma into an ambient highly magnetized plasma capable of supporting Alfvén waves will be presented. The 150 MW laser is pulsed at the same 1 Hz repetition rate as the plasma in a highly reproducible experiment. The laser beam impacts a solid target such that the initial plasma burst is directed across the ambient magnetic field. The interaction results in the production of intense shear and compressional Alfvén waves, as well as large density perturbations. The waves propagate away from the target and are observed to become plasma column resonances. The magnetic fields of the waves are measured with a 3-axis inductive probe. Spatial patterns of the magnetic fields associated with the waves and density perturbations are acquired at over 10,000 spatial locations and as a function of time. Measurements are used to estimate the coupling efficiency of the laser energy and kinetic energy of the dense plasma into wave energy. The shear wave generation mechanism is due to field-aligned return currents, which replace fast electrons escaping the initial blast. *INDEX TERMS:* 7831 Space Plasma Physics: Laboratory studies; 7513 Solar Physics, Astrophysics, and Astronomy: Coronal mass ejections; 7871 Space Plasma Physics: Waves and instabilities; 2111 Interplanetary Physics: Ejecta, driver gases, and magnetic clouds; 7524 Solar Physics, Astrophysics, and Astronomy: Magnetic fields; *KEYWORDS:* Alfven waves, diamagnetic cavities, supersonic expansion, Alfven wings, high beta plasmas, cross-field expansion, current systems

Citation: Gekelman, W., M. Van Zeeland, S. Vincena, and P. Pribyl, Laboratory experiments on Alfvén waves caused by rapidly expanding plasmas and their relationship to space phenomena, *J. Geophys. Res.*, *108*(A7), 1281, doi:10.1029/2002JA009741, 2003.

1. Introduction

[2] There are many instances, both naturally occurring and man-made, in which a dense plasma expands into much less dense background plasma. On astrophysical scales there are jets which have extreme conditions and may be modeled in the laboratory using intense lasers. In the past decade, Coronal Mass Ejections [*Low*, 2001] (CMEs) from the Sun have been detected and are now the subject of a great deal of study. CMEs have wreaked havoc on the Earth. Properly speaking, high-speed plasma moving from the Sun to the Earth is termed ''fast ejecta.'' Complex ejecta are fast ejecta which have associated magnetic fields which vary rapidly in direction and in which counter-streaming electrons have been observed [*Burlaga et al.*, 2001]. One cause of complex ejecta has been postulated to be the interaction of one or more CMEs. CMEs may also evolve into structures such as flux ropes [*Chen and Garren*, 1993; *Chen*, 1997] (sometimes called magnetic clouds) which are observed by satellites near the Earth. Models of flux ropes have similar magnetic geometries as those of complex ejecta. When these structures impact the Earth's magnetosphere geomagnetic storms can occur [*Gosling et al.*, 1991]. When such storms arrive at the Earth they can induce currents in power lines and transformers, which, in turn, can disrupt power grids [*Kappenman et al.*, 1997]. A geomagnetic storm in 1989 caused a system wide power failure in Quebec [*Pirjola*, 2000], which resulted in a loss of 20 GW of electrical power to 6 million people. The time from the onset of the problem to the collapse of the system was 90 s. Coupled to this storm was the loss of half the circuitry in a Japanese satellite. A NASA satellite dropped 3 miles from its initial orbit position on onset. In 1997 another storm left the U.S. Telstar communications satellite inoperable (cost $200 million). A recent storm on Bastille Day (14 July) 2000 [*Knowles et al.*, 2001] destroyed a communications satellite, which resulted in at least one day in which bank ATMs and credit card transactions virtually ceased.

[3] In the 1962 Starfish experiment a 1.4-megaton bomb was detonated 400 km above the South Pacific [*Colgate*, 1965]. Shortly afterwards an electrical generating station in

0148-0227/03/2002JA009741$09.00

Hawaii was severely damaged. It was conjectured that this was due to induced fields that coupled to the power grid and caused a transformer to fail. The fields originated in an Alfvén wave driven by the expanding plasma.

[4] If a satellite is electrically conductive and moves across the ambient magnetic field, it will experience induced charge separation. Currents then travel along the field lines in the background plasma to neutralize the space charge. These currents were postulated to close via the generation of ''Alfvén wings'' which are combinations of Alfvén wave propagation along the ambient field and plasma flow in the frame of the satellite. The current closure in this model depends on cross-field conductivity and was used to successfully calculate the drag on the Echo I satellite [*Drell et al.*, 1965]. Alfvén (or whistler) wings may be the source of pitch angle scattering of electrons by the motion of Amalthea (a satellite of Jupiter which may be conductive) in Jupiter's radiation belts [*De Pater et al.*, 1997]. Alfvén waves may have been triggered when the comet Shoemaker-Levy 9 struck Jupiter in 1994, when impact generated hot spots in the planet's ionosphere moved upward into the surrounding plasma [*De Pater and Brecht*, 2000].

[5] There have been chemical releases in the Earth's ionosphere which have triggered wave activity [*Bernhardt et al.*, 1987] and unexpected plasma motion [*Haerendel et al.*, 1985; *Lui et al.*, 1986; *Papadopoulos and Lui*, 1986; *Cheng*, 1987; *Chapman*, 1989]. An experimental program began in 1990 was designed, in part, to study the interaction of the ambient plasma with a localized dense chemical release. The Combined Release and Radiation Effects Satellite (CRESS) placed varying amounts of barium (and other atoms with low ionization energies) into the ambient plasma at altitudes from 517 to 33,553 km at fairly low latitudes [*Bernhardt*, 1991]. Plasma motion could be tracked from the ground using telescopes. The initial plasma density was larger than that of the background and there was an ambient magnetic field. Diamagnetic cavities were produced just as in our laboratory experiments and were measured with instruments onboard the satellite. In two cases in which barium was released at the highest altitude the magnetic field was completely excluded from the bubble [*Bernhardt et al.*, 1987]. The released plasma cloud was observed to move sideways across the magnetic field. This motion was termed ''skidding.'' A recent three-dimensional computer simulation [*Delamere et al.*, 2001] shows Alfvén waves propagating along the background magnetic field and transferring momentum away from the Barium and into the ambient plasma.

[6] To simulate these situations in the laboratory an expanding plasma is generated when an aluminum target is struck by a high power laser ($P \approx 10^{11}$ W/cm^2). The target is immersed in a uniform, magnetized plasma capable of supporting Alfvén waves. A dense Al plasma, initially millimeters in diameter and nearly at solid density then expands outward from the target surface. In this earliest stage the plasma collisonality exceeds the electron cyclotron frequency and neither the electrons nor Al ions are magnetized. The initial laser-produced plasma (lpp) freely expands across the magnetic field. Diamagnetic currents are set up in the lpp which expel the background magnetic field. At this time the structure is termed a ''magnetic bubble'' [*Ripin et al.*, 1993]. The bubble radius, without the presence of collisions, is obtained by equating the expelled magnetic field to the initial particle energy and is $R_b = \left[3\mu_0\left(E_{lpp}/\pi B_0^2\right)\right]^{1/3}$ (this is derived for expansion from a flat surface). Here E_{lpp} is the kinetic energy of the laser-produced plasma. In our experiment the bubble radius is about 4 cm less than 1/12th the background plasma column diameter. The expanding bubble experiences a deceleration ($v_\perp^2/2R_b$) and stops expanding at $\tau = (2R_b)/v_\perp$, which is approximately 0.53 μs in the laboratory. Subsequent to bubble formation the lpp becomes magnetized and expands along the magnetic field as a tube of plasma. In these experiments fast ions are produced in the lpp and their Larmor radius is always greater than the bubble radius (for charge states less than 3).

[7] There are many diverse phenomena associated with motion of a dense plasma across and along an ambient magnetic field. The processes can involve the generation of a variety of plasma waves. In this paper we concentrate on Alfvén waves produced by rapidly expanding plasmas. For this to occur the plasma must expand into an ambient background plasma which is magnetized and which can support Alfvén waves. To study these processes in the laboratory and relate them, in some way, to processes in space there are two things that must be considered, scaling and topology. These are discussed next before the experiment and data are presented.

2. Topology

[8] Solar phenomena, our laser plasma experiment, and cloud releases have different magnetic field topologies. If magnetic field lines which are oppositely directed are pushed together, magnetic field line reconnection may occur. This process results in the change of the magnetic topology as well as energy releases. An expanding plasma is accompanied by density and space charge gradients and fast particles and will be the source of plasma waves whether or not there is reconnection. The magnetic topology in flares has not been measured. The only data presently available are detailed measurements at a host of optical wavelengths and X-rays. These can be directly related to electron temperatures and their structure leads to models of what the magnetic fields may be. Satellites have made measurements of the magnetic fields of CMEs [*Mulligan and Russell*, 2001] at isolated locations, which have led to flux rope models. The background magnetic field in the Starfish experiment is well known, but the induced fields in the explosion are not. A great deal of modeling as well as a series of laser-plasma experiments can give us a reasonable guess. The best we can do at the present time is assume these models are correct and in the laboratory try to create similar geometries. Figure 1 shows the magnetic topology of a CME and that of a dense, high-pressure plasma expanding into a background field and ambient plasma. The CME expands across the background dipole field of the Sun.

[9] The conjectured magnetic topology of the CME in Figure 1a is different from the expanding plasma shown in Figure 1b. The magnetic field that emerges from the surface of the Sun is most likely twisted. The twist is attributed to processes which occur below the surface of the Sun and are related to the solar dynamo. As the CME expands away from the solar surface into the background magnetic field, the geometry changes and the CME can become detached,

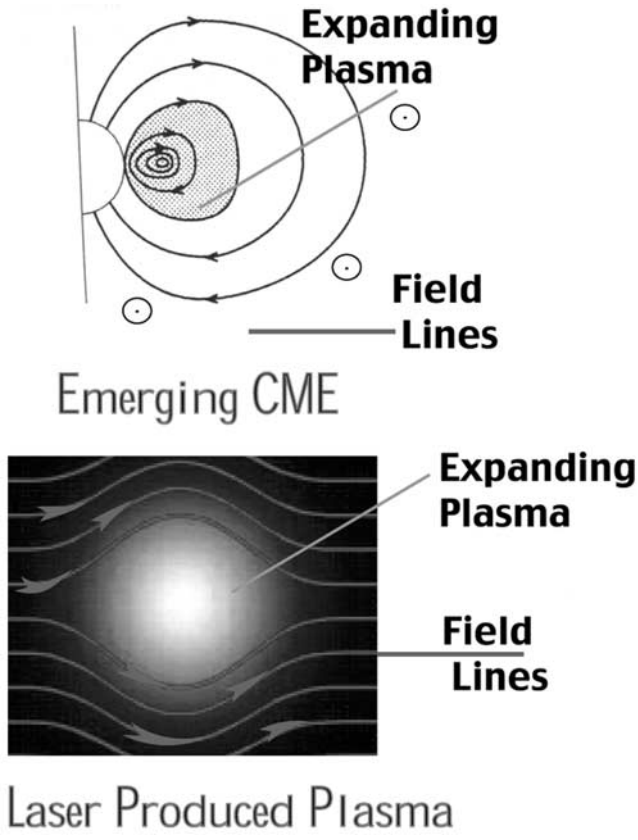

Figure 1. (a) The conjectured magnetic field topology of a coronal mass ejection. The emerging magnetic field is anchored to the highly conducting surface of the Sun. The CME is ejected and moves off to the right into the less dense coronal plasma and background magnetic field (here shown pointing out of the page). (b) A dense localized plasma is caused by a laser target interaction or other means. This dense plasma is surrounded by plasma. The background plasma, in both cases, can support a variety of waves.

presumably as the result of magnetic field line reconnection. In some models the CME is still anchored to the Sun even as it strikes the Earth. The magnetic field within the expanding plasma bubble, on the other hand, is the result of the diamagnetic current superimposed upon the uniform background magnetic field. Although the topologies of the magnetic field in these cases are different, they both represent a large perturbation on the ambient magnetic field as well as currents and, we believe, generate intense wave activity.

3. Scaling

[10] The median CME speeds are 4.5×10^7 cm/s, mean Alfvén speed in the solar corona 10^8 cm/s, ion sound speed 10^7 cm/s. The laboratory numbers are similar $V_{Alfvén} = 2.4 \times 10^7 - 1.2 \times 10^8$ cm/s, and the sound speed is $1 \times 10^5 - 1 \times 10^6$ cm/s, but the spatial scales are vastly different. The parameters are best compared in a table of dimensionless ratios.

[11] The laboratory experiment quoted is the present one and the parameters are calculated when the plasma bubble has expanded to a radius of 4 cm. It is possible to obtain other ranges for these ratios by varying the background magnetic field, density and ion species. The CRESS-G2 Barium release occurred at an altitude of 6180 km and was sunlit. The CME data is for an eruption still close to the sun. Here V_{te} is the electron thermal speed, n is density, and $\beta = (2\mu_0 nKT)/B^2$.

[12] Table 1 compares relevant dimensionless parameters for the laboratory and other cases. The plasma beta is similar in all three cases. In the laboratory case n_{bubble}/n_o is smaller than in the other cases, but this is calculated at the time at which the bubble radius is a maximum. The initial laser produced plasma is several orders of magnitude more dense. If the laboratory ratio were made similar by lowering the background plasma, it could not support Alfvén waves because their wavelength would be too large to fit in the experimental device. The ratio $R_{ci\text{-}lpp}/R_{bubble}$, which compares the expanding plasma's Larmor radius to the bubble size, is dependent on charge state. The value quoted in the table is for $Z = 1$ and serves as an upper limit.

[13] Although the scaling is not perfect, and we do not try to make a 1:1 correspondence with CMEs, CRESS, or the "Starfish," yet it is likely that what occurs in the laboratory will shed light on these events.

4. Experimental Arrangement

[14] The experiments involve a target struck by a laser beam aligned perpendicular to the background magnetic field. A parallel incidence experiment was performed on the original LAPD device [*Gekelman et al.*, 1991] and some results have been previously reported [*Van Zeeland et al.*, 2001]. More experiments are planned for this case in the future. The experiments involving laser incidence across the background field were performed in the upgraded LAPD device. The "new machine," a major upgrade of the original, has an 18 m long plasma column in a background magnetic field which can be as high as 3.5 kG. A larger cathode produces a highly ionized plasma column 60 cm in diameter (200 R_{ci} for a neon plasma at 1.5 kG, $n_e \approx 2 \times 10^{12}$ cm^{-3}, $T_e = 6$ eV, $T_i = 1$ eV in this experiment). The device has 450 access ports, which allow for volumetric mapping of plasma parameters during experiments. Probes and antennas can be inserted and removed while the machine is under vacuum through over sixty vacuum interlocks, many having rotatable flanges for volumetric probe positioning [*Leneman and Gekelman*, 2001] The experimental arrangement is shown in Figure 2.

[15] The experimental sequence is as follows: The plasma is initiated once per second by pulsing the oxide coated cathode negatively with respect to an anode 32 cm away. The discharge current grows to its maximum value in several milliseconds (ms) and is maintained for ≈10 ms.

Table 1. Relevant Dimensionless Parameters for the Laboratory and Other Cases

	Laboratory	CME	CRESS (G2)	Starfish
$V_{cloud}/V_{Alfvén}$	0.3	0.1–2.0	6.7×10^{-4}	5.0
B (background plasma)	3×10^{-4}	4×10^{-4}	3.2×10^{-5}	3×10^{-5}
V_{cloud}/V_{sound}	30	4.5	0.16	2500
$R_{ci\text{-}lpp}/R_{bubble}$	5	10^{-8}	0.03–0.008	10^{-3}
$R_{ci\text{-}back}/R_{bubble}$	0.075	10^{-7}	1.6×10^{-3}	1.4×10^{-2}
n_{bubble}/n_0	15	1×10^4	5–500	250
$V_{te}/V_{Alfvén}$	2	0.9	0.175	0.5

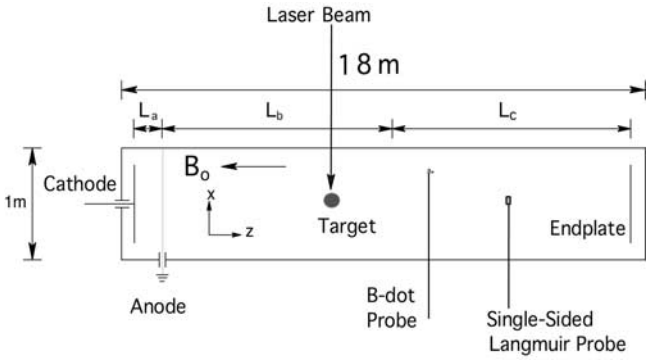

Figure 2. Experimental arrangement when laser is incident perpendicular to the background magnetic field. An Al target is placed in a 18 m long plasma column produced by a DC discharge between a cathode and mesh anode on one end. A 1.5 J (τ = 7 ns, λ = 1 μm) laser beam is incident through a port on one side of the machine. The plasma is confined by a uniform background magnetic field of 1.5 kG. The distances shown are L_a = 50 cm, L_b = 667 cm, L_c = 1033 cm.

In the middle of the discharge a pulse triggers the flash lamps of a 150 MW (τ = 7 ns, E = 1.5 Joule, λ = 1.064 micron) YAG laser, the beam of which enters the device through an antireflection coated window. The laser is focused (dia-spot $\leq$ 0.5 mm) on an Al rod (dia = 1.95 cm) radially centered in the plasma column and 7 m from the cathode. The laser pulse, timing, and plasma conditions are highly reproducible. After the target is struck five times it is rotated until a fresh surface is presented to the laser. Data from the five successive shots are averaged and the detection probe is moved to the next spatial location. Upon a single revolution of the target a second stepping motor lowers the target by a millimeter. A single Al rod lasts for approximately one week ($\approx 1 \times 10^5$ shots). The target is then replaced utilizing a vacuum interlock. The target motion diagnostic probe positioning and data collection are all under computer control.

[16] Magnetic field data were acquired with 3-axis magnetic pickup loops (area = 0.84 cm^2) and density with a Langmuir probe (area = 1 mm^2). Each axis of the magnetic probe is differentially wound and was calibrated in air by measuring its response to an AC current in a long wire. Its frequency response was determined with a network analyzer. The differential probe signals for each component were subtracted (to remove the electrostatic component) and then sent to a high-frequency ($f \leq$ 60 MHz) optical coupler. An electric dipole probe was used to measure whistler and lower hybrid waves and is the subject of a future publication. During the course of data acquisition the probes were moved in planes both parallel and perpendicular to the background axial magnetic field. Data were acquired with a bank of digitizers operating at 4 ns/sample (Δt = 32 μs) and 40 ns/sample rates (Δt = 320 μs) to study both low and high frequency phenomena.

5. Experimental Results

[17] As a means of benchmarking our experiment, initial measurements were made with no background plasma and were in accord with previous experiments by *Dimonte and Wiley* [1991]. A fast ($t_{exposure}$ = 1 ns) gated imager as well as a Faraday cup array was used to record the plasma expansion with and without a background magnetic field. The lpp was found to contain approximately 2.5 $\times$ 10^{15} particles and an initial expansion speed of 1.5 $\times$ 10^7 cm/s normal to the target and 1 $\times$ 10^7 cm/s perpendicular. This is consistent with other experiments done without background plasma, and with various target materials and shapes quoting laser-to-plasma conversion efficiencies of 20–80 percent [*Ripin et al.*, 1980; *Decoste et al.*, 1979].

[18] With no magnetic field, the expansion is self-similar as previously documented. With a background magnetic field, a diamagnetic cavity (magnetic bubble) is formed as discussed in the introduction and the late expansion becomes primarily directed along the magnetic field. The magnetic field diffuses back into the bubble on a time-scale of 1.2 μs, which is 50 times faster than the classical diffusion time $\tau_D = \mu_0 \sigma R^2_{\text{bubble}}$, where σ is the classical conductivity evaluated for a lpp electron temperature of 6 eV with R_b = 0.04 m.

[19] In vacuum a burst of fast electrons leads the expanding dense plasma, and the expansion speed becomes limited by charge separation and ion inertia. In the presence of a dense background plasma the magnetic bubble formation is similar to the vacuum case. The dynamics of the expansion are altered, however, because charges can flow in the background plasma to neutralize the space charge, possibly reducing the diamagnetic effect. We will see that this process is the root of Alfvén wave generation. The laser plasma-plasma interaction occurs on multiple time-scales as illustrated in Table 2.

[20] Fast ions were measured with an energy analyzer in the vacuum case (E = 1 – 4 keV). However velocity analyzers are difficult to use in the presence of background plasma since the Debye length is small $\tau_D \approx 10^{-3}$ cm), and their readings are inaccurate. A burst of fast electrons has been measured with a Langmuir probe. These streaming electrons trigger electron plasma waves, as well as intense lower hybrid waves (S. Vincena et al., Lower hybrid wave generation from a laser-produced plasma, submitted to *Geophysical Research Letters*, 2003). The lower hybrid waves were identified using their dispersion; higher frequency waves were detected at further radial distances at a fixed location downstream from the target. In this work we concentrate on the Alfvén waves as well as large density fluctuations.

[21] In these experiments we acquired magnetic field data at four transverse planes (x–y) and two horizontal planes (x–z). A Langmuir probe $A \cong 1$ mm^2) was used to measure ion saturation current, $I_{sat} \propto n\sqrt{T_e/M_I}$, on four vertical planes. Data were acquired at sampling rates of both 4

Table 2. Time Scales for the Laser Plasma Experiment

Process	Timescale/Frequency
Laser pulse	7 ns, 143 MHz
Fast particle generation	0.01–7 ns, 143Mhz–100 GHz
Langmuir waves	0.07 ns, 15 GHz
Lower hybrid/whistler waves	10–100 ns, 10–100 MHz
Lifetime of diamagnetic bubble	1 μs , 1 MHz
Alfvén waves	1–67 μs, 15 kHz–1 MHz
Ion acoustic waves	10–100 μs, 10 kHz–100kHz

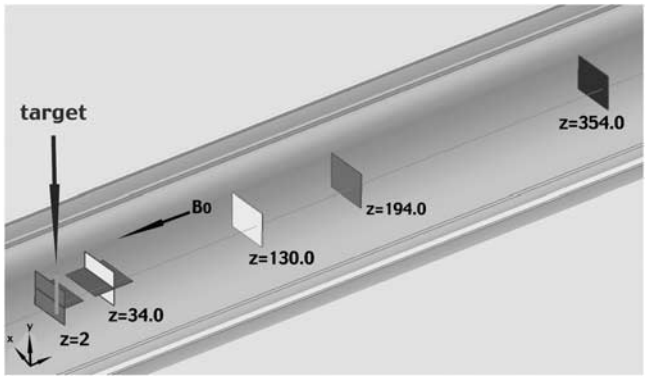

Figure 3. Schematic of the interior of the LAPD device and the data planes within it, drawn to scale. The diagram shows the target and distances to the data planes with respect to the laser impact point. Magnetic field data were acquired on planes z = 2 cm, 34 cm, 130 cm and 194 cm as well as the two horizontal planes. Langmuir probe data were acquired on planes z = 34, 130, 354 cm, and 578 cm (not shown). All distances are in centimeters. The transverse (vertical) planes have dimensions $\Delta x = 25$ cm, $\Delta y = 20$ cm. The horizontal plane which starts at $z = 2$ cm has dimensions $\Delta x = 25$ cm, $\Delta z = 12$ cm. The second horizontal plane which straddles $z = 34$ cm has dimensions $\Delta x = 25$ cm, $\Delta z = 24$ cm. The laser is incident from the left side of the target and comes in at $z = 0$, the target location. The plasma source is located at $z = -8.55$ m.

and 40 ns/sample to capture both fast and slow features. A schematic of the data planes within the machine is shown in Figure 3.

[22] The collected current to the Langmuir probe exposed to the plasma streaming along B_0 is shown as a function of time in Figure 4 at a fixed position in two planes. The probe

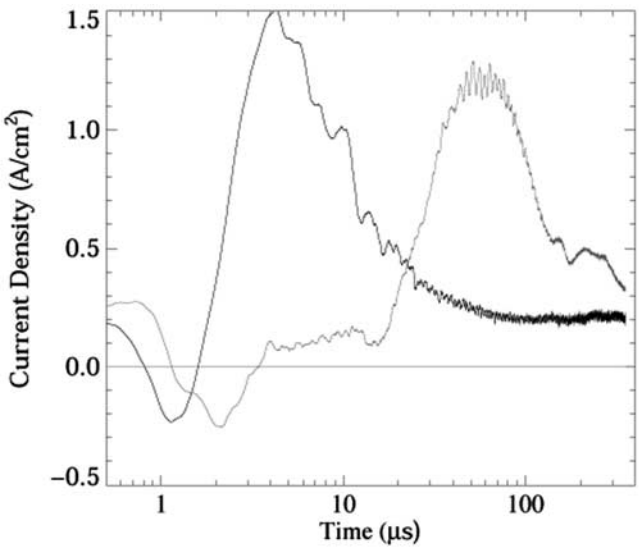

Figure 4. Signal to a Langmuir probe with area of 1 mm^2, which is biased $V_B = -67$ Volts with respect to the anode. The dark curve is for a probe at $z = 34$ cm and the second at $z = 354.0$ cm. Both probes are located at $x = 10$ cm and $y = 2.5$ cm. The laser impact point on the target is located at $x = y = z = 0$.

is biased with respect to the anode to repel electrons with energies less than 67 volts. It is clear that the probe signal in the first few microseconds is dominated by electrons, with a signal arriving later at the further plane. The time of flight between these planes corresponds to a velocity of $\approx 3 \times 10^8$ cm/s.

[23] Initially, fast aluminum ions ($E_{\text{Ion}} \geq 1$ keV) accelerated by the large electric fields of the laser leave the target and move across the magnetic field. They drag some electrons with them ($v_D = 1.5 \times 10^7$ cm/sec, $E_{\text{electron}} \cong 0.3$eV). The drift speed of these electrons is less than that of the background electron thermal speed. A fraction of the electrons released initially jet away from the target along the magnetic field; their number depends upon the density of the background plasma. This makes the lpp plasma near the target positive with respect to the background plasma. If there were no background plasma, the initial field-aligned electrons would be held back by ion inertia, and this would determine the dynamics of the expansion [*Decoste and Ripin*, 1977]. When background plasma is present it responds to the charge imbalance of the lpp cloud. Background electrons stream towards the lpp initially creating a nearly coaxial system. This is illustrated in Figure 5, in

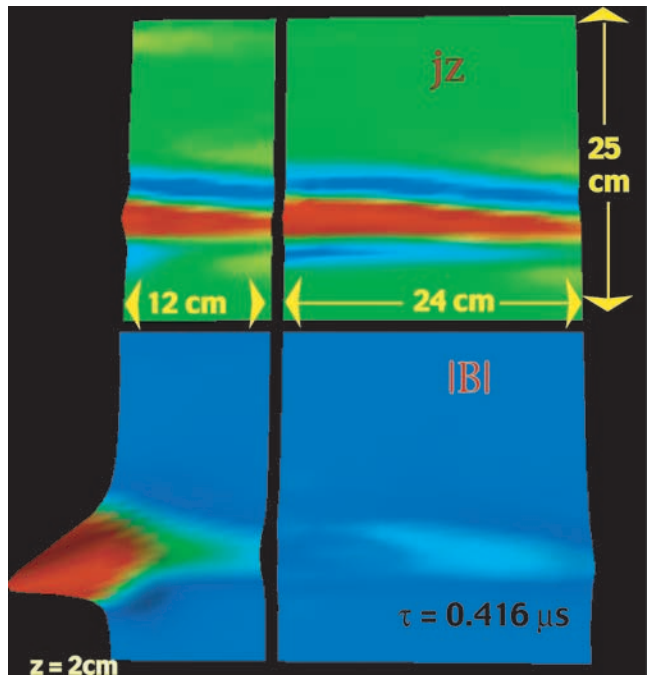

Figure 5. (top) Axial current in two horizontal (x−z) planes. Data were acquired at 663 locations in the plane which has length $\Delta z = 12$ cm and 1275 locations in the plane which has length $\Delta z = 24$ cm. Both planes are at $y = 0$. The red surface denotes electrons moving away from the target and blue electrons streaming toward it (see color bar in Figure 6). (bottom) Magnitude of the measured magnetic field in these planes at the same time. This is the field expelled from the lpp by diamagnetic currents. The constant background magnetic field, B_0, points in the $-z$ direction and is not shown. The data were acquired at intervals of 0.5 cm in the x-direction and 1 cm in the z-direction. It was smoothed over 1 cm^2 area to eliminate noise from taking spatial derivatives.

which the current, j_{z_2} is determined using the measured magnetic field from $\vec{\mathbf{j}} = (1/\mu_0)\nabla \times \vec{\mathbf{B}}$. The determination of j_z is exact in the vertical planes; in the horizontal planes, however, only one part of the axial current ($\partial_x B_y$) can be calculated from the data. In the first microseconds of the expansion the coaxial currents imply $B_x \approx 0$, $\partial_y B_x \approx 0$. In time the currents become complicated and this assumption breaks down. With this caveat we display (Figure 5) the current and the magnitude of the perturbed magnetic field taken 412 ns after the target is struck.

[24] The data indicate that a current system associated with fast electrons is set up quickly, well before Alfvén waves are generated. The return currents are associated with background electrons, which flow toward the lpp to neutralize space charge, as well as inductive current. The system inductance at early times is determined by the coaxial geometry of the electrons leaving the lpp and the coaxial return current. In the first half microsecond the inductive electric field is large and can contribute as much to the return current as the charging of the lpp. The cross-field currents, which close the circuit, are due to the ion polarization drift

$$j_\perp = ne\frac{1}{\omega_{cI}B}\frac{dE_\perp}{dt}.$$

In a plasma which can support Alfvén waves, changes in current systems are broadcast by these waves and after a wave period $E_\perp$ becomes part of the Alfvén wave field.

[25] A short time later (t = 0.496 μs) the magnetic disturbance has grown and becomes visible further away, at z = 1.3 m. This is illustrated in Figure 6, which shows both current (j_z) and magnetic field. The magnetic field due to the diamagnetic currents is clearly visible. It points outward from the target and in the center it points in the $+z$ direction. The background field is in the $-z$ direction, and they cancel near the target. The field expulsion is due to diamagnetic currents within the lpp cloud. In a previous experiment by *Dimonte* [1992], Faraday rotation was used to directly measure the expelled field. At the time for which Figure 6 was generated the axial currents are nearly coaxial; however, some structure is evident in the second horizontal plane. The assumption on the calculation of j_z made above is still probably valid since the derived current matches that on the vertical plane, where no such assumption was made.

[26] In the presence of background plasma the lpp electrons and ions are not strongly coupled. The lpp produces a dense puff of Al ions, which initially move away from the target at a characteristic speed of $v_{\|-Al} \cong 1 \times 10^7$ cm/s, $v_{\perp-AL} \cong 1.5 \times 10^7$ cm/s. This unimpeded motion across the magnetic field continues until the ions move by an ion gyroradius ($R_{Al} \cong 19$ cm, $Z = 1$), which corresponds to an initial directed energy of 4 keV. This is a plasma jet, directed across the strong background field and has been observed in previous experiments [*Mostovych et al.*, 1989]. The mechanism responsible for the cross-field electron motion is an $\mathbf{E_p} \times \mathbf{B_0}$ drift, where $\mathbf{E_p}$ is the polarization electric field. A surface charge appears on the lpp due to the oppositely directed ion and electron Larmor motion [*Schmidt*, 1966]. This is the cause of the polarization electric field ($E_p = v_\perp B_0 = 225$ V/cm). As the ions expand across the magnetic field, electrons from the lpp cloud also move along the background magnetic field, B_0, from new

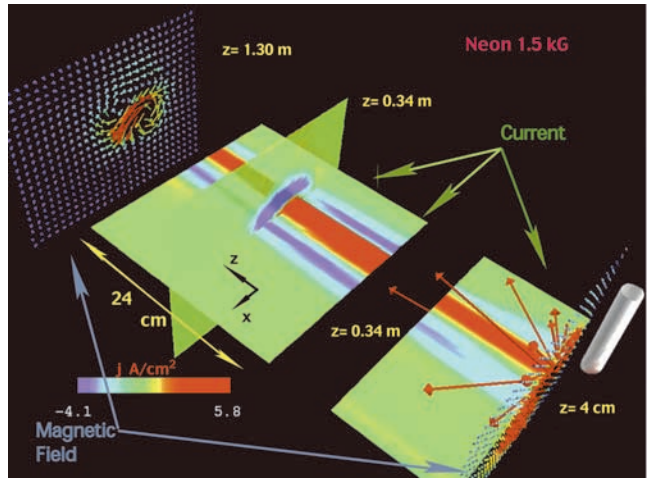

Figure 6. Axial current shown on three planes as a surface plot and magnetic field vectors measured on two additional planes. The target is 2 cm to the rear of the rightmost vertical plane, t = 0.496 μs. Note the constant background magnetic field is not shown in this figure. The data were acquired at 1-cm intervals along z and 0.5 cm intervals in the transverse planes.

radial locations. The emerging space charge is continuously neutralized by electron return current, which the background plasma supplies. The generation of Alfvén waves comes about as the field-aligned current ($I = n_{lpp}ev_\|A_\perp \cong 150$ A) is neutralized by cross-field ion polarization current. This current system forms an effective antenna, which radiates the waves. *Borovsky* [1987] has done a theoretical analysis of a plasma which is injected across an ambient magnetic field. The experiment and his model have many features in common. In his model the $q\vec{\mathbf{v}} \times \vec{\mathbf{B}}$ force deflects the charges in opposite directions and the outgoing stream is polarized. The charges also move along the background field and form a current system, which is closed by the polarization drift. The current system in this model produces "Alfvén wings" [*Goertz and Boswell*, 1979], waves launched by the streaming plasma. The "wings" are shear Alfvén waves and the Alfvén waves couple the parallel electric fields and currents to the perpendicular fields and currents. Estimates of the cross-field current for our parameters given by Borovsky are larger, by a factor of five, than what is needed to close the field-aligned current, but the wave amplitudes in the experiment drop along the ambient magnetic field and the boundaries are not as simple as those in the model.

[27] After the cross-field expansion stops, the ion motion is principally along B_0. The ion plume is shown as an isosurface in Figure 7. Figure 7 is generated from spatially interpolated data and illustrates the three dimensional expansion of the ion cloud. At this time (4.0 μs) its center has drifted across the field by Δx = 10 cm and it has expanded along the magnetic field by 75 cm. The ions displayed in the isosurface represent a current of 0.9 A/cm^2 which corresponds to a density of 3×10^{13} cm^{-3}, assuming $Z = 1$ (singly charged Al, Te = 6 eV). It is likely that the aluminum target ions are multiply charged so this is an upper density limit. The parallel drift speed of the aluminum

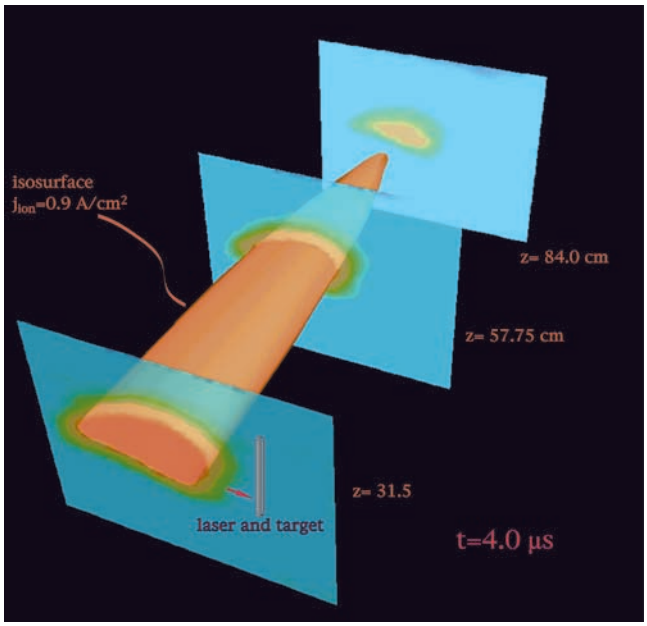

Figure 7. Isosurface of constant ion density taken 4 μs after the target is struck. The target has been illustrated to scale for reference. The single-sided probe data from the vertical planes shown in Figure 5 was interpolated to the rear two planes shown here. The perpendicular planes have dimensions Δx = 25 cm, Δy = 20 cm.

ions is 1×10^7 cm/s, which is $0.2V_{Alfven}$ and twenty times the ion acoustic speed of the background neon plasma.

[28] Aside from the fast particles and large density perturbation, the lpp is a source of wave activity. The initial fast electrons are a source of lower hybrid and whistler waves. These waves move away from the target in cones with major axis aligned along the ambient field. Waves with higher frequencies are observed at larger cone angles in accord with the cold plasma dispersion relation [*Schmidt*, 1966]. In time of the order of 1 μs the current system due to electrons leaving the target, and background electrons flowing in to neutralize the space charge have generated waves. Thermal electrons (T_e = 6 eV, $v_e = 1 \times 10^8$ cm/s) have been able to move 1 m and fast target electrons ($E >$ 100 eV, $v > 4 \times 10^8$ cm/s) have approached the end of the machine. The wave pattern 1.34 m from the target is shown in Figure 8.

[29] The maximum wave magnetic field is 5 G at this distance, and $(\delta b_{wave})/B_0 = 3.3 \times 10^{-3}$. The current channel on the right in Figure 8a is due to electrons leaving the target (which is vertical and positioned to the right of the field pattern). The current channel on the left is due to return currents, which have, at this time, lost their coaxial symmetry because the lpp has moved to the left. The velocity of an Alfvén wave in these experimental conditions is 5.2×10^7 cm/sec and it takes 12.8 μs to travel 6.67 m to the closest end of the machine, which is terminated with the anode. One would expect an Alfvén field line resonance [*Mitchell et al.*, 2002] to form on the machine transit time which is 32.7 μs. The wave pattern distinctly changes by t = 24.2 μs as illustrated in Figure 9.

[30] The large axial currents directly associated with the plasma expansion have dropped to one tenth of their peak

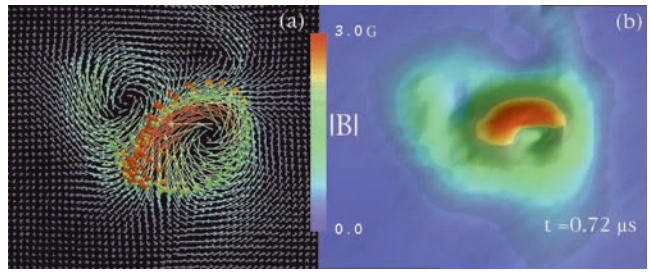

Figure 8. Data perpendicular to the background magnetic field at axial location z = 194 cm. (a) Measured wave fields at τ = 0.72 μs. (b) The magnitude of the wave magnetic field. The wave magnetic field is averaged over five shots at each of the 2091 locations ($\delta x = \delta y$ = 0.5 cm). Data were taken in a neon plasma with a 1.5 kG background magnetic field. The axes are as in Figure 3; the x axis points from left to right.

value at 5 μs and are nearly gone at 10 μs. At time t = 24 μs the lpp current is no longer present and the current system associated with Figure 9 is due entirely to the Alfvén wave. The wave patterns shown in Figure 8 evolve in time to that of Figure 9. Note that the data in Figures 8 and 9 are unfiltered and contain all frequencies. The mode, which occurs at late time, is a global mode. The interaction, in fact, produces a spectrum of modes in the Alfvénic regime. This can be seen in the spectrum shown in Figure 10. These experiments were repeated for a background magnetic field of 1.0 kG and the results were essentially the same.

[31] When the temporal data of the magnetic field is digitally filtered at this frequency at each location, the inverse transform yields the spatial pattern as a function of time (within Nyquist limits). The pattern at 15 kHz is shown in Figure 11. Note that this mode is strikingly like that of Figure 9, which indicates that at this time this contains most of the wave energy. This global m = 0 mode is seen at every transverse plane on which data were acquired. It corresponds to a shear mode with parallel wavelength $\lambda_{\|} \cong V_A/f$ = 34.5 m, which is twice the column length. The spectrum also shows higher frequency shear modes. The modes below the cyclotron frequency are shear Alfvén waves in the host medium, that is the background neon plasma. The higher frequency modes ($f > f_{ci}$) on the other hand are spatially localized with the dense cloud of aluminum ions.

[32] Figure 12a a shows the ion saturation current to a $1mm^2$, flat probe facing the target and located 1.3 m away.

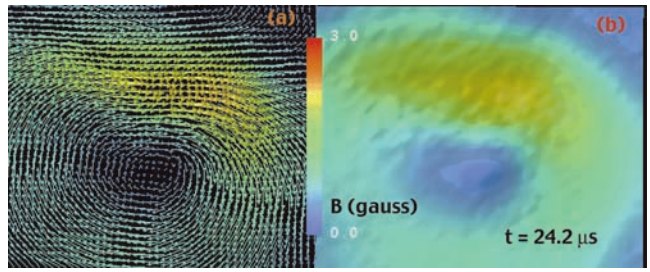

Figure 9. Wave magnetic field (a) and its magnitude (b) at t = 24.2 μs. The experimental conditions are the same as in Figure 8.

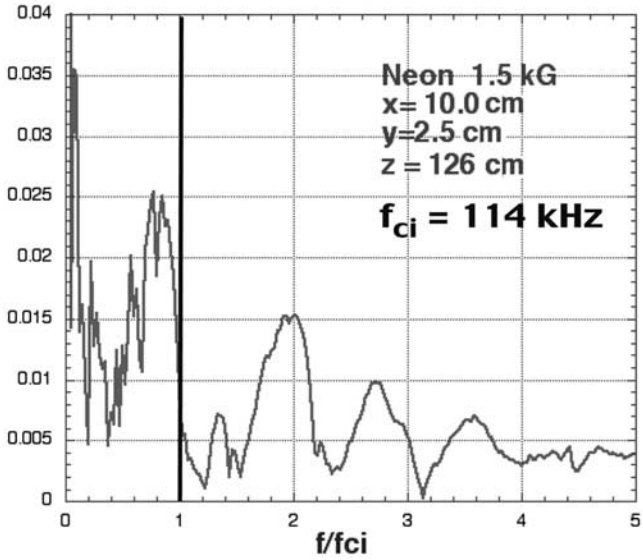

Figure 10. Power spectrum of the fluctuations of one component of the wave magnetic field. (B_y is the vertical component). The laser impact site is located at $x = y = z = 0$. Shear waves occupy the region below $f/f_{ci} = 1$, delineated by the vertical line.

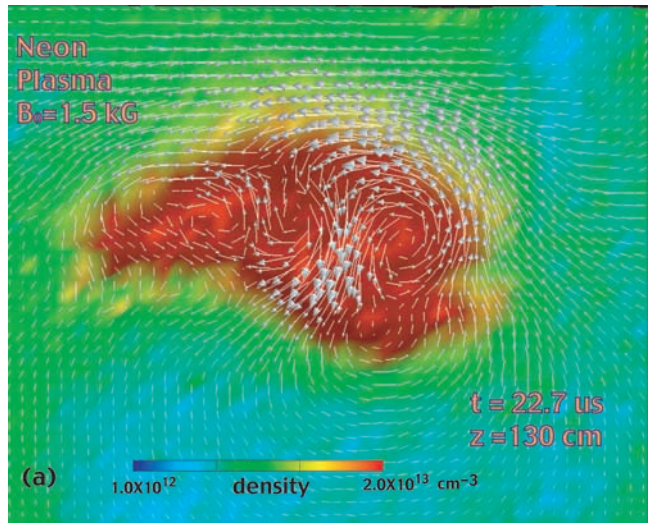

Figure 12a. Color map of the density and vector magnetic field. The vector magnetic field is Hanning filtered at frequency 250 kHz, $\Delta f = 50$ kHz, $z = 1.3$ m from the target and taken 22.7 μs after the laser hits the target. The red object in the center is the aluminum plasma. It is surrounded by a neon plasma, which has an average density of 2×10^{12} cm^{-3}. Note the faint vertical depression on the upper right side of the image. This is the perturbation caused by the target.

The ion saturation current depends on plasma density and the electron temperature, $I_{sat} \propto n_0\sqrt{T_e}$. It is assumed that at the relatively late time ($t = 22.7$ μs) at which these data were acquired, that the electron temperature of both the lpp and background plasma are approximately equal ($\tau_{ee}/\tau \ll 1$). The variations in the ion saturation current therefore reflect primarily those in the plasma density. The Al plasma is ten times denser than the background neon plasma and shows up in red in the center of the figure. Also shown is the digitally filtered ($f = 250$ kHz $= 2.19\ f_{ci}$) vector magnetic field in this plane, at the same time. The magnetic fluctuations at this frequency are spatially associated with the denser plasma. It is possible these modes are fast Alfvén waves associated with density gradients. Waves below the ion cyclotron frequency have been clearly observed in and around density cavities [*Maggs and Morales*, 1996; *Burke et al.*, 2000] and have been studied theoretically [*Penano et al.*, 1997]. These modes have density fluctuations associated with them as well as magnetic field fluctuations.

[33] Figure 12b shows the spatial relation between the density fluctuations ($(\delta n)/n \approx 1\%$) and magnetic field fluctuations ($(\delta B)/B \approx 0.02\%$), both filtered at 250 kHz. Although these seem to be associated with each other on the

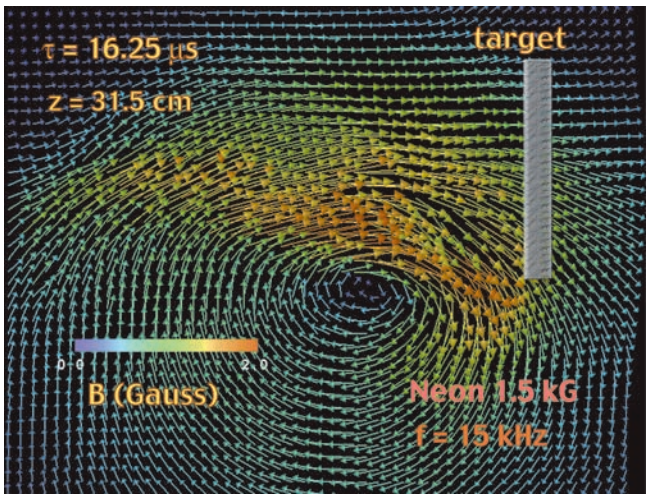

Figure 11. Digitally filtered ($f = 15$ kHz $= 0.13\ f_{ci}$) magnetic field at $t = 16.25$ μs after the target was struck. The position of the target with respect to the pattern is shown as a gray rectangle.

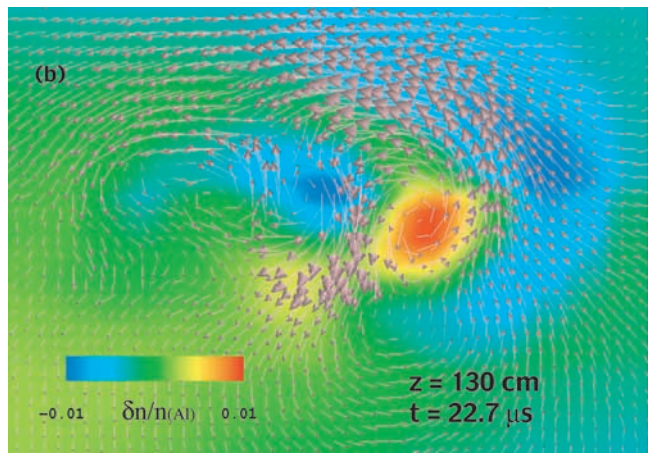

Figure 12b. Density fluctuations and vector magnetic field at 250 kHz. The largest density fluctuations are 1% of the maximum density of the Aluminum plasma at this spatial location $\delta z = 126$ cm.

upper right hand part of the panel, the evidence is not compelling. These higher-frequency waves will be explored in future experiments, but their magnetic field amplitude is well below that of the shear waves. Instability in a transverse jet in a strong magnetic field but with no background plasma has been seen before [*Mendel and Olsen*, 1975; *Ripin et al.*, 1984]. In an experiment with a barium target in a 10 kG magnetic field, the surface of transverse plasma plume was observed to break into field aligned striations.

[34] One likely candidate discussed in that work was the lower hybrid drift instability, but it was never confirmed. The transverse structure instabilities seen in this experiment and others are important and fascinating and will be explored in future work.

6. Summary and Conclusions

[35] The production and expansion of the dense plasma is associated with many transient phenomena. A diamagnetic cavity is formed from which the background magnetic field is expelled. Additionally, energetic ions are generated, as well as fast electrons, which stream along the magnetic field away from the lpp cloud. Recently, whistler and Langmuir waves have been observed inside magnetic clouds by detectors on the WIND spacecraft [*Moullard et al.*, 2001]. These waves propagated along the magnetic field and were associated with measured electron loss-cone distribution functions. The source of the superthermal electrons was not pinned down. In this experiment, waves were not measured within the cloud, only those that escaped.

[36] As reported here, the dense cloud develops a space charge as a result of the streaming electrons and the background plasma responds by generating electron return currents. These current systems generate a variety of waves. This series of laboratory experiments has shown that intense Alfvén waves are generated in a spectrum of frequencies. In addition, initial plasma motion across the magnetic field results in the generation of focused jets. As the cloud expands across the magnetic field it continually produces field-aligned currents which in turn generate new Alfvén waves on new magnetic field lines. Integration of the magnetic energy, in the frequency band we explored and measured on all planes show that about seventy percent of the wave energy resides in shear Alfvén waves.

[37] There are a great variety of natural processes such as coronal mass ejections, high-altitude chemical releases, astrophysical jets, magnetic clouds, and complex ejecta which involve these types of expansions. The boundary conditions as well as other details of these events vary on a case-by-case basis, and they may not even be well known in some cases. It is here where laboratory experiments can play an important role, perhaps more important than numerical simulations. The case for using laser plasma experiments to simulate astrophysical phenomena was made over 40 years ago by *Dawson* [1964]. Dawson points out that the scaling should be reasonable, although if a very specific phenomenon is not being modeled, approximate scaling will do. In the laboratory the initial conditions are well known and can be tailored. A variety of data (density, temperature, flow, magnetic, and electric fields) can be acquired in great detail in space and time. These may be integrated to form a scenario, which in this case is the interplay between fast particles, currents, and waves. This in turn could cause a space plasma physicist to consider alternate explanations, reinterpret data, or plan new measurements on upcoming missions.

[38] **Acknowledgments.** The authors wish to thank George Morales and Jim Maggs for many informative discussions and Guy Dimonte for his collaboration on the earlier work. We also wish to thank the ONR (grant N00014-97-1-0167), DOE (grant DE-FG03-98ER54494), and NSF for their support in this research. We also acknowledge the expert technical assistance of Marvin Drandell. Finally, the authors wish to thank the two referees for their valuable suggestions.

[39] Shadia Rifai Habbal thanks Ellen Zweibel and another referee for their assistance in evaluating this paper.

References

Burlaga, L. F., R. M. Skoug, C. W. Smith, D. F. Webb, H. T. Zurbuchen, and A. Reinard, Fast ejecta during the ascending phase of solar cycle 23: ACE observations, 1998–1999, *J. Geophys. Res.*, *106*, 20,957–20,977, 2001.

Bernhardt, P. A., Probing the magnetosphere using chemical releases from the combined release and radiation effects satellite, *Phys. Fluids B*, *4*, 2249–2256, 1991.

Bernhardt, P., R. A. Roussel-Dupre, M. B. Pongratz, G. Haerendel, A. Valenzuela, D. A. Gurnett, and R. R. Anderson, Observations and theory of the AMPTE magnetotail barium releases, *J. Geophys. Res.*, *92*, 5777–5794, 1987.

Borovsky, J., Limits on the cross-field propagation of streams of cold plasma, *Phys. Fluids*, *30*, 2518–2526, 1987.

Burke, A., G. Morales, and J. Maggs, Spontaneous fluctuations of a temperature filament in a magnetized plasma, *Phys. Rev. Lett.*, *84*, 1451–1454, 2000.

Chapman, S. C., On the bulk motion of ion clouds formed by the AMPTE solar wind/magnetosheath releases, *J. Geophys. Res.*, *94*, 227–240, 1989.

Chen, J., Theory of prominence eruption and propagation: Interplanetary consequences, *J. Geophys. Res.*, *101*, 27,499–27,519, 1997.

Chen, J., and D. Garren, Interplanetary magnetic clouds: Topology and driving mechanism, *Geophys. Res. Lett.*, *20*, 2319–2322, 1993.

Cheng, A. F., Transverse deflection and dissipation of small plasma beams and clouds in magnetized media, *J. Geophys. Res.*, *92*, 55, 1987.

Colgate, S., The phenomenology of the mass motion of a high-altitude nuclear explosion, *J. Geophys. Res.*, *70*, 3161, 1965.

Dawson, J., On the production of plasma by giant pulse lasers, *Phys. Fluids*, *7*, 981–987, 1964.

Decoste, R., and B. H. Ripin, High energy ions from a Nd-laser produced plasma, *Appl. Phys. Lett.*, *31*, 68–70, 1977.

Decoste, R., S. E. Bodner, B. H. Ripin, E. A. McClean, S. P. Obenschain, and C. M. Armstrong, Ablative acceleration of laser irradiated thin-foil targets, *Phys. Rev. Lett.*, *42*, 1673–1677, 1979.

Delamere, P. A., D. W. Swift, and H. C. Stenbaek-Nielsen, An explanation of the ion cloud morphology in the CREES plasma injection experiment, *J. Geophys. Res.*, *106*, 21,289–21,295, 2001.

De Pater, I., and S. Brecht, SL9 imapcts: VLA high resolution observations at $\lambda = 20$ cm, *Icarus*, *151*, 1–24, 2000.

De Pater, I., M. Schulz, and S. H. Brecht, Synchrotron evidence for Amalthea's influence on Jupiter's electron radiation belt, *J. Geophys. Res.*, *102*, 22,043–22,064, 1997.

Dimonte, G., A magneto-optic imaging probe for continuous magnetic field profiles, *Rev. Sci. Instrum.*, *63*, 5151–5153, 1992.

Dimonte, G., and L. Wiley, Dynamics of exploding plasmas in a magnetic field, *Phys. Rev. Lett.*, *67*, 1755–1758, 1991.

Drell, S. D., H. M. Foley, and M. A. Ruderman, Drag and propulsion of large satellites in the ionosphere: An Alfvén propulsion engine in space, *J. Geophys. Res.*, *70*, 3131–3145, 1965.

Gekelman, W., H. Pfister, Z. Lucky, J. Bamber, D. Leneman, and J. Maggs, Design, construction and properties of the Large Plasma Research Device—the LAPD at UCLA, *Rev. Sci. Instrum.*, *62*, 2875–2883, 1991.

Goertz, C. K., and R. W. Boswell, Magnetosphere-ionosphere coupling, *J. Geophys. Res.*, *84*, 7239–7245, 1979.

Gosling, J. T., D. J. Mcomas, J. L. Phillips, and S. J. Bame, Geomagnetic activity associated with the Earth passage of interplanetary shock disturbances and coronal mass ejections, *J. Geophys. Res.*, *96*, 7831–7839, 1991.

Haerendel, G., et al., The Li/Ba release experiments of the ion release module, *IEEE Trans. Geosci. Remote Sens.*, *23*, 253–258, 1985.

Kappenman, J., L. Zanetti, and W. Radasky, Geomagnetic storms can threaten electric power grids, *Earth Space*, *9*, 9, 1997.

Knowles, S. H., J. M. Picone, S. E. Thonnard, and A. C. Nicholas, The effect of atmospheric drag on satellite orbits during the Bastille Day event, *Sol. Phys.*, *204*, 387–397, 2001.

Leneman, D., and W. Gekelman, A novel angular motion vacuum feedthrough, *Rev. Sci. Instrum.*, *72*, 3473–3474, 2001.

Low, B. C., Coronal mass ejections, magnetic flux ropes, and solar magnetism, *J. Geophys. Res.*, *106*, 25,141–25,163, 2001.

Lui, A. T., C. C. Goodrich, A. Mankofsky, and K. Papadopoulos, Early time interaction of lithium ions with the solar wind in the AMPTE mission, *Geophys. Res.*, *91*, 1333, 1986.

Maggs, J., and G. Morales, Magnetic fluctuations associated with field-aligned striations, *Geophys. Res. Lett.*, *23*, 633–636, 1996.

Mendel, C., Jr., and J. Olsen, Charge-separation electric fields in laser plasmas, *Phys. Rev. Lett.*, *34*, 859–862, 1975.

Mitchell, C., J. Maggs, and W. Gekelman, Field line resonances in a cylindrical plasma, *Phys. Plasmas*, *9*, 2909–2918, 2002.

Mostovych, A., B. Ripin, and J. Stamper, Laser-produced jets: Collimation and instability in strong transeverse magnetic fields, *Phys. Rev. Lett.*, *62*, 2837–2840, 1989.

Moullard, O., D. Burgess, C. Salem, A. Mangeney, D. E. Larson, and S. D. Balle, Whistler waves, Langmuir waves and single loss cone electron distributions inside a magnetic cloud: Observations, *J. Geophys. Res.*, *106*, 8301–8313, 2001.

Mulligan, T., and C. T. Russell, Multispacecraft modeling of the flux rope structure of interplanetary coronal mass ejections: Cylindrically symmetric versus nonsymmetric topologies, *J. Geophys. Res.*, *106*, 10,581–10,596, 2001.

Papadopoulos, K., and A. T. Lui, On the initial motion of artificial comets in the AMPTE releases, *Geophys. Res. Lett.*, *13*, 925–927, 1986.

Penano, J. R., G. Morales, and J. Maggs, Properties of drift waves in a filamentary density depletion, *Phys. Plasmas*, *4*, 555–565, 1997.

Pirjola, R., Geomagnetically induced currents during magnetic storms, *IEEE Trans. Plasma. Sci.*, *28*, 1867–1873, 2000.

Ripin, B. H., R. R. Whitlock, F. C. Yang, S. P. Obenschain, E. A. McLean, and R. Decoste, Laser plasma interaction and ablative acceleration of thin foils at $10^{12} - 10^{15}$ W/cm^2, *Phys. Fluids*, *23*, 1012, 1980.

Ripin, B. H., E. A. McLean, C. K. Manka, C. Pawley, J. A. Stamper, T. A. Peyser, A. N. Mostovych, J. Grun, A. B. Hassam, and J. D. Huba, Large Larmor-radius interchange instability, *Phys. Rev. Lett.*, *59*, 2299–2302, 1984.

Ripin, B. H., J. D. Huba, E. A. McLan, C. K. Manka, T. Peyser, H. R. Burris, and J. Grun, Sub Alfvénic plasma expansion, *Phys. Fluids*, *5*, 3491–3506, 1993.

Schmidt, G., *The Physics of High Temperature Plasmas*, Academic, San Diego, Calif., 1966.

Van Zeeland, M., W. Gekelman, and S. Vincena, Production of Alfvén waves by a rapidly expanding dense plasma, *Phys. Rev. Lett.*, *87*, 105001.1-105001-4, 2001.

W. Gekelman, P. Pribyl, S. Vincena, and M. Van Zeeland, Department of Physics and Astronomy, University of California, Los Angeles, Los Angeles, CA 90045, USA. (gekelman@physics.ucla.edu; pribyl@ucla.edu; vincena@physics.ucla.edu; mav@physics.ucla.edu)